Solution processable donor materials based on thiophene and triphenylamine for bulk heterojunction solar cells†

Jongchul Kwon,[a] Woochul Lee,[a] Ji-young Kim,[c] Seunguk Noh,[b] Changhee Lee[b] and Jong-In Hong*[a]

Received (in Montpellier, France) 28th August 2009, Accepted 15th January 2010
First published as an Advance Article on the web 23rd February 2010
DOI: 10.1039/b9nj00431a

Solution processable and thermally stable donor materials 2,5-bis[4-(*N*,*N*-diphenylamino)styryl] thiophene (**1**) and 2,5-bis[4-(*N*,*N*-diphenylamino)styryl]-2,2′-bithiophene (**2**) were synthesized for bulk heterojunction solar cells, which consist of a thiophene, or bithiophene and triphenylamine unit linked with conjugated bonds. The best device performance, optimized at **1**:PCBM = 1:3 and **2**:PCBM = 1:4, exhibited the maximum open circuit voltages of 0.56 and 0.51 V, short circuit currents of 1.33 and 1.88 mA cm^{-2}, and power conversion efficiencies of 0.23 and 0.34%, respectively, under simulated AM 1.5 solar irradiation at 100 mW cm^{-2}.

Introduction

Since the first introduction of organic solar cells (OSCs) based on donor–acceptor heterojunctions by Tang,[1] the development of organic solar cells has attracted considerable attention in recent years, due to their easy synthesis, low cost and easy device fabrication. Researchers have focused on improving the power conversion efficiency of the devices using new materials.[2,3] In recent years, the power conversion efficiency of organic solar cells has been steadily enhanced by the use of various device fabrication methods.[4]

Small organic molecules based on oligothiophenes and acenes[5] have often been used as organic semiconductors due to their good charge transport ability. However, since these materials are known to be oriented perpendicularly on the substrate, OSC device fabrication using these materials results in a reduction in absorption of the incident light as well as charge transport to the electrode. Also, it is difficult to form a uniform film by solution processes with these small organic molecules because they can be easily crystallized in organic solvents.[6,7]

To overcome these problems, Shirota *et al.* and Roncali *et al.* reported 3-dimensional (3-D) star- and propeller-shaped triphenylamine (TPA) derivatives[6,7] in which the three phenyl groups are not in the same plane. Furthermore, solution processable triphenylamine derivatives were widely investigated for their electroluminescence, hole transport and OSC potential due to their good charge transport ability and good solubility in organic solvents.[6–8] Also, thiophene derivatives have been extensively investigated for their utility as organic thin film transistors (OTFTs),[9] organic light emitting diodes (OLEDs)[10] and OSCs,[11–12] due to their good charge transport ability and good thermal stability.

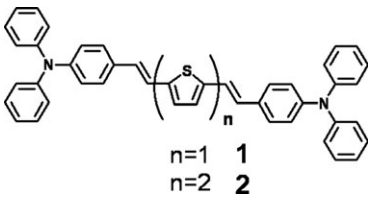

Fig. 1 Molecular structures of **1** and **2**.

In this paper, we report that donor materials **1** and **2**, consisting of a thiophene and triphenylamine units linked with conjugated bonds, can be successfully utilized to fabricate new bulk heterojunction OSC devices by spin coating of a blended solution of **1** or **2** and [6,6]-phenyl C_{61}-butyric acid methyl ester (PCBM) (Fig. 1). As a result, the best device performance optimized, at **2**:PCBM = 1:4, exhibited an open circuit voltage (V_{oc}) of 0.51 V, short circuit current (I_{sc}) of 1.88 mA cm^{-2} and power conversion efficiency (PCE) of 0.34%, under simulated AM 1.5 solar irradiation at 100 mW cm^{-2}.

Experimental section

Reagent and materials

2,5-Dibromothiophene, 5,5′-dibromo-2,2′-bithiophene, palladium acetate ($Pd(OAc)_2$), tetrabutylammonium bromide (TBAB), *N*,*N*-dimethylformamide (DMF), [6,6]-phenyl C_{61}-butyric acid methyl ester (PCBM), 4,7-diphenyl-1,10-phenanthroline (Bphen), and 2,9-dimethyl-4,7-diphenyl-1,10-phenanthroline (BCP) were purchased from Aldrich and LMC. Poly(3,4-ethylenedioxythiophene)-poly(styrenesulfonate) (PEDOT:PSS) was purchased from Baytron. Biphenyl-(4-vinylphenyl)amine (**3**) was prepared according to the literature procedure.[13] Analytical thin layer chromatography was performed using Kieselgel 60F-254 plates from Merck. Column chromatography was

[a] *Department of Chemistry, College of Natural Sciences, Seoul National University, Seoul 151-747, Korea. E-mail: jihong@snu.ac.kr; Fax: +82-2-889-1568; Tel: +82-2-880-6682*
[b] *School of Electrical Engineering and Computer Science, Interuniversity Semiconductor Research Center, Seoul National University, Seoul 151-742, Korea. E-mail: chlee7@snu.ac.kr*
[c] *Interdisciplinary Graduate Program in Nanoscience and Nanotechnology, Seoul National University, Seoul 151-742, Korea*
† Electronic supplementary information (ESI) available: UV, PL, device data, TGA. See DOI: 10.1039/b9nj00431a

carried out on Merck silica gel 60 (70–230 mesh). All solvents and reagents were commercially available and used without further purification unless otherwise noted.

Instruments

^{1}H and ^{13}C NMR spectra were recorded using an Advance 300 or 500 MHz Bruker spectrometer in $CDCl_3$. ^{1}H NMR chemical shifts in $CDCl_3$ were referenced to $CHCl_3$ (7.27 ppm), and ^{13}C NMR chemical shifts in $CDCl_3$ were reported relative to $CHCl_3$ (77 ppm). UV-vis spectra were recorded on a Beckman DU 650 spectrophotometer. Mass spectra were obtained using a MALDI-TOF mass spectrometer from Bruker. Fluorescence spectra were recorded on a Jasco FP-7500 spectrophotometer. Cyclic voltammetry (CV) was performed using a CH instruments 660 electrochemical analyzer. AFM images of spin-coated blended thin films were obtained using a PSIA XE-100 advanced scanning microscope. The film thickness of the organic layers were measured using alphastep (KLA Tencor). Decomposition temperatures (T_d) were obtained using a thermal gravimetric analyzer (TGA) from a Q–5000–IR TGA instrument. Glass transition temperatures (T_g) were obtained using a DSC–Q–1000 instrument.

Syntheses

2,5-Bis[4-(*N*,*N*-diphenylamino)styryl]thiophene (1). A mixture of 2,5-dibromothiophene (808 mg, 3.34 mmol), compound **3** (1.84 mg, 6.68 mmol), palladium acetate (33.1 mg, 0.204 mmol), tetrabutylammonium bromide (TBAB, 215 mg, 0.66 mmol) and sodium acetate (1.42 g, 17.3 mmol) in DMF was heated at 70 °C for 24 h. After cooling to room temperature, the solvent was evaporated under high vacuum and the reaction mixture was extracted with dichloromethane. The organic phase was washed with water and dried over Na_2SO_4. The solvent was evaporated to give a reddish product, which was applied to column chromatography on silica gel using ethyl acetate and hexane as eluent, and recrystallized from dichloromethane and hexane to give a reddish solid product (yield: 700 mg, 34%). ^{1}H NMR (300 MHz, $CDCl_3$): δ (ppm) 7.35 (d, 9 Hz, 4H), 7.29 (t, 15 Hz, 8H), 7.18 (d, 6 Hz, 2H), 7.14 (d, 9 Hz, 4H), 7.06 (t, 9 Hz, 4H), 7.01 (d, 9 Hz, 8H), 6.92 (s, 2H), 6.87 (s, 2H). ^{13}C NMR (125 MHz, $CDCl_3$): δ (ppm) 147.5, 142.3, 131.2, 129.4, 127.9, 127.6, 127.3, 126.7, 125.6, 124.6, 123.9, 120.4. Mass: calcd. for $C_{44}H_{34}N_2S$ $[M]^+$ 622.2443, HR-mass: 622.2444.

2,5-Bis[4-(*N*,*N*-diphenylamino)styryl]-2,2′-bithiophene (2). A mixture of 5,5′-dibromo-2,2′-bithiophene (835 mg, 2.57 mmol), compound **3** (1.40 mg, 5.15 mmol), palladium acetate (25.5 mg, 0.15 mmol), TBAB (165 mg, 0.51 mmol) and sodium acetate (1.09 g, 13.3 mmol) in DMF was heated at 70 °C for 24 h. After cooling to room temperature, the solvent was evaporated under high vacuum and the reaction mixture was extracted with dichloromethane. The organic phase was washed with water and dried over Na_2SO_4. The solvent was evaporated to give a reddish product, which was applied to column chromatography on silica gel using ethyl acetate and hexane as eluent, and recrystallizated from dichloromethane and hexane to give a reddish solid product (yield: 800 mg, 44%). ^{1}H NMR (300 MHz, $CDCl_3$): δ (ppm) 7.35 (d, 9 Hz, 4H), 7.30 (t, 15 Hz, 8H), 7.14 (d, 15 Hz, 4H), 7.07 (t, 6 Hz, 4H), 7.05 (d, 9 Hz, 8H), 6.95 (d, 3 Hz, 2H), 6.93 (d, 3 Hz, 2H), 6.82 (s, 2H), 6.79 (s, 2H). ^{13}C NMR (125 MHz, $CDCl_3$): δ (ppm) 147.6, 142.5, 135.9, 131.1, 129.5, 128.1, 127.4, 126.9, 125.1, 124.7, 124.2, 123.6, 123.3, 120.1. Mass: calcd. for $C_{48}H_{36}BrN_2S_2$ $[M]^+$ 704.2320, HR-mass: 704.2316.

Results and discussion

1 and **2** were synthesized by a Heck coupling reaction between biphenyl-(4-vinylphenyl)amine (**3**)[13] and 2,5-dibromothiophene or 5,5′-dibromo-2,2′-bithiophene, respectively (Scheme 1).

Fig. 2 and ESI, Fig. S1† show the UV and PL spectra of **1** and **2** in CH_2Cl_2, neat films, and the blended film of **1** and **2**:PCBM = 1:1. The absorption spectra of **1** and **2** in CH_2Cl_2 show three main absorption bands, with λ_{max} at 281, 408, 441 nm, and 271, 386, 461 nm, in which peaks at 281 and 271 nm originate from the triphenylamine unit, and peaks at 441 and 461 nm originate from the olighthiophene core, respectively. The PL spectra of **1** and **2** in CH_2Cl_2 show an

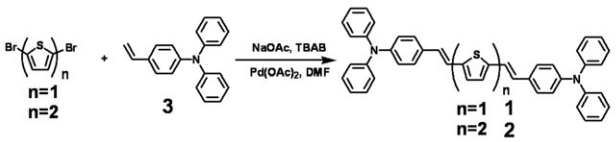

Scheme 1 Synthesis of **1** and **2**.

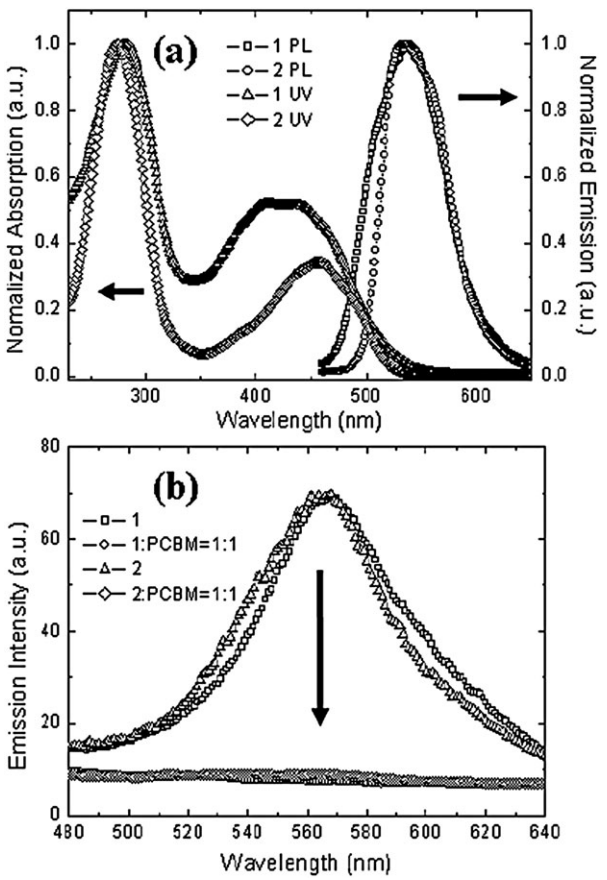

Fig. 2 UV and PL spectra of **1** or **2** in CH_2Cl_2 (a) and **1** or **2** neat solid film (b) and the blended film of **1** or **2**:PCBM = 1:1 (b).

Table 1 Photophysical and electrochemical data for **1** and **2**

	Absorption (λ_{nm}) ($\varepsilon \times 10^5$/M cm)[a]	Emission (λ_{nm})[a]	HOMO[b]/eV	LUMO[c]/eV	ΔE[d]/eV
1	281(5.80), 408(3.00), 441(2.95) (solution) 282, 410, 442 (film)	538 (solution) 565 (film)	5.00	2.54	2.46
2	271(10.5), 386(1.35), 461(3.60) (solution) 272, 386, 461 (film)	538 (solution) 565 (film)	5.01	2.47	2.54

[a] The absorption and emission spectra were measured in 0.02 mM CH_2Cl_2 solution and quartz solid film. [b] HOMO energy levels were determined in CH_2Cl_2 solution (0.1 M $TBAPF_6$) *vs.* AgCl. HOMO = $E_{1/2}^{ox}$ + 4.49 eV. [c] LUMO energy levels were calculated from the cross-sectional wavelength between absorption and emission spectra. [d] ΔE = HOMO − LUMO.

emission peak at 538 nm. The absorption spectra of **1** and **2** in solid films show absorption bands with λ_{max} at 282, 410, 442 nm, and 272, 386, 461 nm, respectively. The PL spectra of **1** and **2** in solid films show an emission peak at 565 nm. In solid films, the PL spectra of **1** and **2** were red-shifted by about 27 nm in comparison with the CH_2Cl_2 solution, due to the self-aggregation and intermolecular interaction[9b] of **1** and **2** (Fig. 2a, ESI Fig. S1†, and Table 1). The PL spectra of the **1** and **2**:PCBM = 1 : 1 blended films indicate that the PL spectra of **1** and **2** were significantly quenched by PCBM (Fig. 2b). That means that an intermolecular photoinduced charge transfer (PICT) and energy transfer process from the excited state of **1** and **2** to PCBM occurred.[8,14] In this blended film of **1** or **2**/PCBM, **1** and **2** were used as the electron donor material, and PCBM as the electron acceptor material. This photoinduced charge transfer process is similar to the case of a conducting conjugated polymer and fullerene blend system.[14]

The electrochemical properties of **1** and **2** were measured by cyclic voltammetry in CH_2Cl_2. This electrochemical experiment was referenced with respect to Ag/AgCl as the reference electrode at room temperature and then calibrated to a standard hydrogen electrode (SHE) using ferrocene/ferrocenium (Fc/Fc^+). Dichloromethane solutions for cyclic voltammetry contained a glassy carbon working electrode, a platinum wire counter-electrode, and 0.1 M tetra-*n*-butylammonium hexafluorophosphate ($TBAPF_6$) as a supporting electrolyte. The cyclic voltammograms of **1** and **2** show a less reversible oxidation process when compared to that associated with the generation of the cation radical. The oxidation potential energies of **1** and **2** are observed at $E_{1/2}$ = 0.68 and 0.70 V *vs.* SHE, respectively (Fig. 3a and b). The HOMO energy levels of **1** (−5.00 eV) and **2** (−5.01 eV) are calculated from $E_{1/2}$ after correction of the vacuum energy level (4.49 eV) (Table 1). The oxidation potential energy of **2** is slightly higher than that of **1** due to the increased thiophene linker and longer conjugation length. The LUMO energy levels of **1** (−2.54 eV) and **2** (−2.47 eV) are calculated from the cross-sectional wavelength between the absorption and emission spectra (Table 1).

The thermal stability of **1** and **2** were investigated using thermal gravimetric analysis (TGA). The thermal decomposition temperatures (T_d) were 412 °C for **1** and 431 °C for **2** (ESI, Fig. S4 and S5†). Both **1** and **2** exhibited high thermal stability. The differential scanning calorimetry (DSC) data showed that the glass transition temperatures (T_g) were 116 °C for **1** and 180 °C for **2** (Fig. S6 and S7†).

Devices based on organic layers were fabricated by spin coating and evaporation. A 30 nm thick film of PEDOT:PSS was used as a hole injection layer. A 45 nm thick film of active

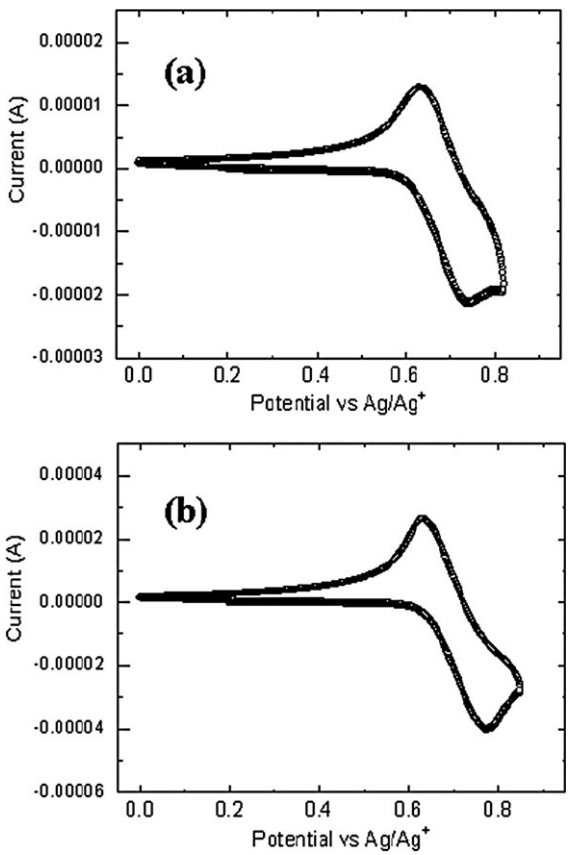

Fig. 3 Cyclic voltammogram of 1.0 mM **1** (a) and **2** (b) in CH_2Cl_2 solution. Scan rate is 0.2 V s^{-1}.

layers was prepared by spin coating an *o*-dichlorobenzene solution of donor (**1** or **2**) and acceptor (PCBM) at different weight ratios (pure, 1 : 1, 1 : 2, 1 : 3, 1 : 4, w/w) on the PEDOT:PSS layer. Next, a 5 nm thick Bphen or BCP layer, as an exciton blocking layer (EBL), was evaporated. Finally, a 100 nm thick aluminium layer was evaporated onto the Bphen layer. The current–voltage (*I–V*) measurements for the devices were performed on a Keithley 237 instrument. The device performances were characterized under uniform illumination (AM 1.5 G illumination intensity of 100 mW cm^{-2}) using a solar simulator. The light intensity at each wavelength was calibrated using the standard Si solar cell as a reference.

In order to investigate the device performances of **1** and **2**, three types of device were fabricated. The first one was the single component device based on pure **1** and **2** as donor; the second was the bilayer heterojunction device based on **1** or **2** as donor and C_{60} as acceptor; the third was the bulk

heterojunction device based on **1** or **2** as donor and PCBM as acceptor. Fig. 4 and ESI, Fig. S3 and S8† show the *I–V* curves of single component, bilayer, and bulk heterojunction devices based on **1** and **2**, respectively. Single component devices based on pure **1** and **2** exhibit very low power conversion efficiency values, open circuit voltages (0.018, 0.007 V) and short circuit currents in comparison with bulk heterojunction devices using **1** or **2**/PCBM, due to the inefficient photoinduced charge transfer and charge separation.[8,14] Also, bilayer devices of **1** and **2**/C_{60} (**1** or **2**: 10 nm, C_{60}: 35 nm) show low power conversion efficiencies of 0.004 and 0.007%, due to inefficient charge separation (ESI, Fig. S8†). However, the power conversion efficiency of bulk heterojunction devices using **1** or **2**:PCBM = 1:1 is significantly higher than those of the single component devices based on pure donors **1** and **2**, and bilayer devices based on **1** and **2**/C_{60}, due to efficient photoinduced charge transfer and charge separation. Therefore, compared with single component devices, bilayer devices and bulk heterojunction devices are much more efficient.[8] It is also evident that bulk heterojunction devices are much more efficient than bilayer devices due to efficient charge separation and charge transport.

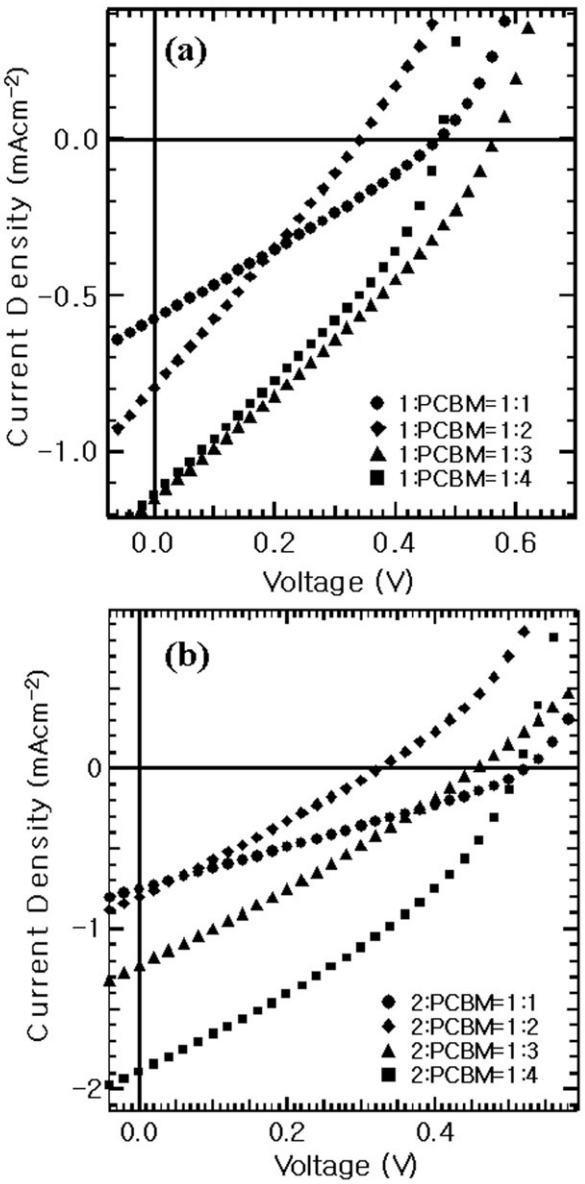

Fig. 4 *I–V* curves of bulk heterojunction devices based on **1** (a) or **2** (b) and PCBM at different weight ratios (1:1, 1:2, 1:3, 1:4) under simulated AM 1.5 solar irradiation at 100 mW cm^{-2}.

In order to achieve optimum device performance, bulk heterojunction devices using **1** or **2**/PCBM were fabricated, and their weight ratios were varied from 1:1 to 1:4. Fig. 4 and Table 2 show the device performances of bulk heterojunction devices based on **1** or **2** and PCBM at different ratios (1:1, 1:2, 1:3, 1:4). In the case of both **1** and **2**, device data exhibited a similar device performance due to their similar molecular structures. At low PCBM concentrations, in the case of **1** or **2**:PCBM = 1:1, the power conversion efficiencies of the devices are 0.08 and 0.11%. Similarly, in the case of **1** or **2**:PCBM = 1:2, the power conversion efficiencies of the devices are the same, at 0.07%. As the PCBM concentration increases, on the other hand, in the case of **1** or **2**:PCBM = 1:3, the power conversion efficiencies of the devices are increased *ca.* 2 times, to 0.23 and 0.15%. In the case of **1** or **2**:PCBM = 1:4, the power conversion efficiencies of the devices are 0.18 and 0.34% (Table 2). As a result, in the case of both **1** and **2**, by increasing the PCBM concentration from 1:1 to 1:4, the power conversion efficiency of the devices are similarly increased *ca.* 2–3 times due to efficient photoinduced charge transfer and charge separation *via* homogeneous film morphology. The overall device data based on **1** or **2** are summarized in Table 2.

In order to examine the dependence of the performance on the film thickness, we fabricated bulk heterojunction devices with different thicknesses of the active layer. Fig. 5 shows the *I–V* curves of bulk heterojunction devices with different active layer thicknesses. At 20 nm thickness of **1** and **2**, the power conversion efficiencies of the devices are 0.08 and 0.07%. At 40 nm thickness of **1** and **2**, the power conversion efficiencies of the devices are slightly increased to 0.10 and 0.13%. The 100 nm thick layers of **1** and **2** show maximum power conversion efficiencies of 0.14 and 0.15%. On the other hand, as the thickness of **1** and **2** was increased further to 200 nm, the devices exhibited slightly reduced power conversion efficiencies

Table 2 Device performance of single component devices based on pure **1** and **2**, bilayer solar cells based on **1** or **2** and C_{60}, and bulk heterojunction solar cells based on **1** or **2** and PCBM with different ratios (1:1, 1:2, 1:3, 1:4) under simulated AM 1.5 solar irradiation at 100 mW cm^{-2}

Active layer	V_{oc}/V	I_{sc}/mA cm^{-2}	FF (%)	PCE (%)
Pure **1**	0.018	0.00035	—	—
1:C_{60}	0.70	0.03	18	0.004
1:PCBM = 1:1	0.34	0.85	27	0.08
1:PCBM = 1:2	0.47	0.57	27	0.07
1:PCBM = 1:3	0.56	1.33	30	0.23
1:PCBM = 1:4	0.46	1.2	31	0.18
Pure **2**	0.007	0.000086	—	—
2:C_{60}	0.76	0.05	15	0.007
2:PCBM = 1:1	0.52	0.75	27	0.11
2:PCBM = 1:2	0.34	0.79	26	0.07
2:PCBM = 1:3	0.45	1.22	27	0.15
2:PCBM = 1:4	0.51	1.88	34	0.34

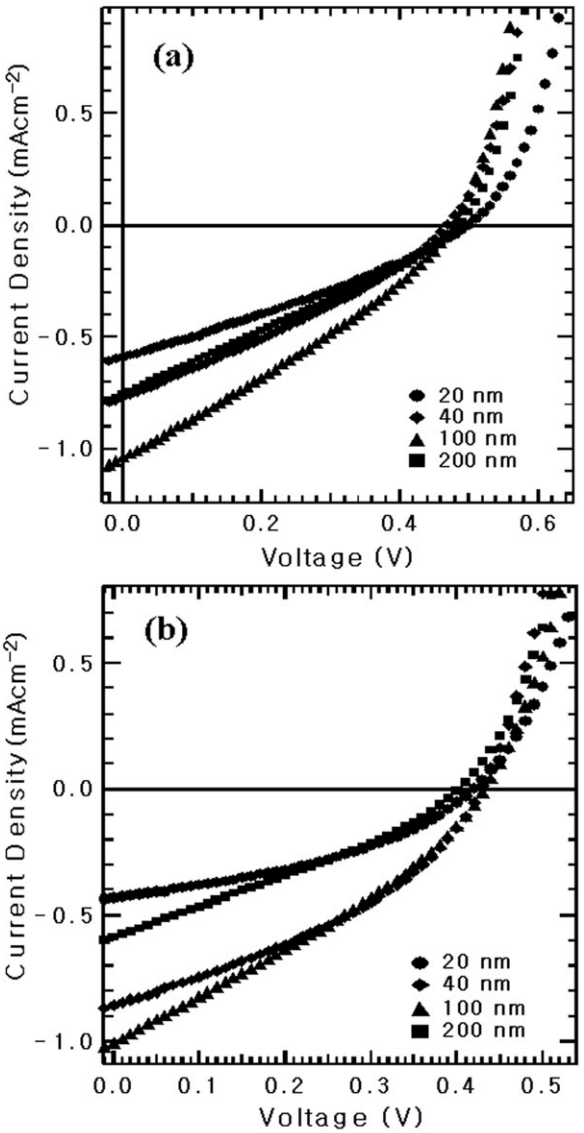

Fig. 5 *I–V* curves of OSCs with different active layer thicknesses of **1**:PCBM = 1:3 (a) and **2**:PCBM = 1:4 (b) under simulated AM 1.5 solar irradiation at 100 mW cm^{-2}.

Table 3 Device performance based on **1**:PCBM = 1:3 and **2**:PCBM = 1:4 with different active layer thicknesses under simulated AM 1.5 solar irradiation at 100 mW cm^{-2}

1 or **2**:PCBM = 1:3 or 1:4	V_{oc}/V	I_{sc}/mA cm^{-2}	FF (%)	PCE (%)
1/PCBM (20 nm)	0.49	0.59	29	0.08
1/PCBM (40 nm)	0.47	0.76	30	0.10
1/PCBM (100 nm)	0.47	1.03	30	0.14
1/PCBM (200 nm)	0.48	0.75	27	0.10
2/PCBM (20 nm)	0.41	0.42	39	0.07
2/PCBM (40 nm)	0.42	0.85	37	0.13
2/PCBM (100 nm)	0.42	1.08	33	0.15
2/PCBM (200 nm)	0.42	0.64	33	0.09

of 0.10 and 0.09%. The change in the thickness of **1** and **2** from 20 to 100 nm in the active layer increased the power conversion efficiencies from 0.08 and 0.07% to 0.14 and 0.15%, respectively. The overall device data based on **1** or **2** are summarized in Table 3.

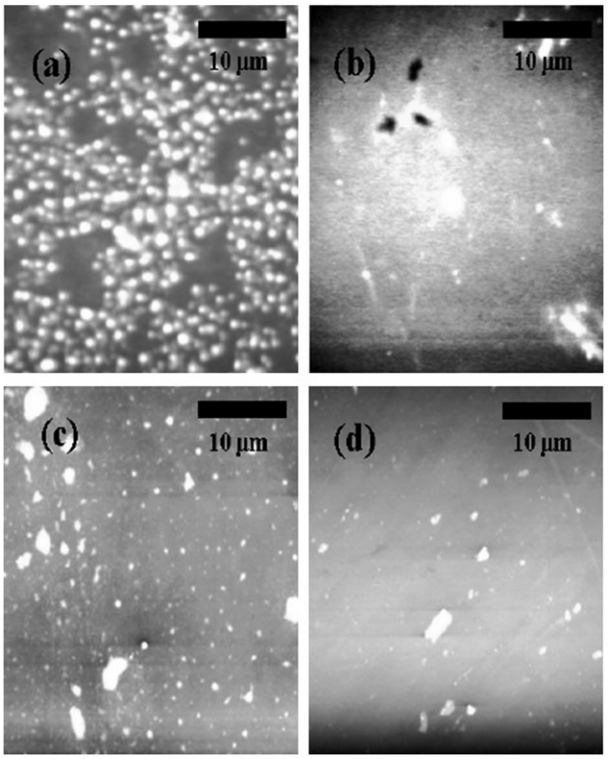

Fig. 6 AFM images of the **1**:PCBM = 1:1 blended solid film (a) and **1**:PCBM = 1:3 blended solid film (b), **2**:PCBM = 1:1 blended solid film (c) and **2**:PCBM = 1:4 blended solid film (d).

We assume that the poor device performance of **1** or **2**:PCBM = 1:1 devices is due to poor morphology, heterogeneous film, and aggregate formation.[15] In order to explain the device performance difference using the **1** or **2**/PCBM blend system, we investigated the morphology of these **1** or **2**/PCBM blended films by atomic force microscopy (AFM).[15] The AFM images of the blended films of **1** or **2**/PCBM are shown in Fig. 6. The morphology of **1** or **2**:PCBM = 1:1 blended films exhibits the formation of many aggregates, and heterogeneous films (Fig. 6a and c), which is likely due to the donor–donor interaction at relatively high concentration of donors **1** and **2**. The poor open circuit voltages, short circuit currents, and power conversion efficiencies of **1** or **2**:PCBM = 1:1 are most likely due to the poor morphology resulting from aggregation of **1** or **2**/PCBM. On the other hand, the morphologies of **1**:PCBM = 1:3 and **2**:PCBM = 1:4 blended films exhibit continuous, homogeneous and good film morphology in comparison with **1** or **2**:PCBM = 1:1 blend solid films (Fig. 6b and d). Thus, at this ratio, they exhibited maximum power conversion efficiency. Therefore, at a higher concentration of PCBM, the power conversion efficiency of the devices increases *ca.* 2–3 times in comparison with low concentrations of PCBM, due to good, continuous, and homogeneous morphology.[8,15]

Conclusions

In conclusion, we have developed solution processable and thermally stable new donor materials **1** and **2**, which consist of

thiophene and triphenylamine units linked with conjugated bonds. The bulk heterojunction devices were fabricated by spin coating the blended solution of **1** or **2** and PCBM at different weight ratios (1 : 1, 1 : 2, 1 : 3, 1 : 4, w/w). Compared with single component devices and bilayer devices, the bulk heterojunction devices using **1** or **2**/PCBM were more efficient. The best device performance is optimized at **2** : PCBM = 1 : 4; the maximum open circuit voltage, short circuit current, and power conversion efficiency value of the device exhibited 0.51 V, 1.88 mA cm^{-2}, and 0.34%, respectively, under simulated AM 1.5 solar irradiation at 100 mW cm^{-2}. **1** and **2**, based on triphenylamine and thiophene derivatives, can be useful as donor materials.

Acknowledgements

This study was supported by the KOSEF grant funded from the MEST of Korea for the Center for Next Generation Dye-sensitized Solar Cell (No. 2009-0063376) and the Seoul R&BD Program (10543). We also acknowledge the BK21 fellowship grant to W.L.

References

1 C. W. Tang, *Appl. Phys. Lett*., 1986, **48**, 183–185.
2 (*a*) G. P. Kushto, W. Kim and Z. H. Kafafi, *Appl. Phys. Lett*., 2005, **86**, 093502; (*b*) K. L. Mutolo, E. I. Mayo, B. P. Rand, S. R. Forrest and M. E. Thompson, *J. Am. Chem. Soc*., 2006, **128**, 8108.
3 (*a*) Y. Shao and Y. Yang, *Adv. Mater*., 2005, **17**, 2841; (*b*) M. T. Lloyd, A. C. Mayer, S. Subramanian, D. A. Mourey, D. J. Herman, A. V. Bapat, J. E. Anthony and G. G. Malliaras, *J. Am. Chem. Soc*., 2007, **129**, 9144; (*c*) L. Valentini, D. Bagnis, A. Marrocchi, M. Seri, A. Taticchi and J. M. Kenny, *Chem. Mater*., 2008, **20**, 32.
4 J. Xue, S. Uchida, B. P. Rand and S. R. Forrest, *Appl. Phys. Lett*., 2004, **85**, 5757.
5 (*a*) J. E. Anthony, *Chem. Rev*., 2006, **106**, 5028–5048; (*b*) J. E. Anthony, *Angew. Chem., Int. Ed*., 2008, **47**, 452–483.
6 (*a*) Y. Shirota, *J. Mater. Chem*., 2000, **10**, 1; (*b*) Y. Shirota, *J. Mater. Chem*., 2005, **15**, 75; (*c*) T. Noda, I. Imae, N. Noma and Y. Shirota, *Adv. Mater*., 1997, **9**, 239; (*d*) T. Noda, H. Ogawa, N. Noma and Y. Shirota, *Adv. Mater*., 1997, **9**, 720.
7 (*a*) S. Roquet, A. Cravino, P. Leriche, O. Alévêque, P. Frère and J. Roncali, *J. Am. Chem. Soc*., 2006, **128**, 3459–3466; (*b*) A. Cravino, S. Roquet, P. Leriche, O. Alévêque, P. Frère and J. Roncali, *Chem. Commun*., 2006, 1416–1418; (*c*) A. Cravino, S. Roquet, O. Alévêque, P. Frère and J. Roncali, *Chem. Mater*., 2006, **18**, 2584.
8 (*a*) C. He, Q. He, X. Yang, G. Wu, C. Yang, F. Bai, Z. Shuai, L. Wang and Y. Li, *J. Phys. Chem. C*, 2007, **111**, 8661–8666; (*b*) C. He, Q. He, Y. He, Y. Li, F. Bai, C. Yang, Y. Ding, L. Wang and J. Ye, *Sol. Energy Mater. Sol. Cells*, 2006, **90**, 1815–1827; (*c*) K. Li, J. Qu, B. Xu, Y. Zhou, L. Liu, P. Peng and W. Tian, *New J. Chem*., 2009, **33**, 2120.
9 (*a*) C. D. Dimitrakopoulos and P. Malenfant, *Adv. Mater*., 2002, **14**, 99; (*b*) M.-C. Um, J. Jang, J. Kang, J.-P. Hong, D. Y. Yoon, S. H. Lee, J.-J. Kim and J.-I. Hong, *J. Mater. Chem*., 2008, **18**, 2234.
10 (*a*) A. Kraft, A. C. Grimsdale and A. B. Holmes, *Angew. Chem., Int. Ed*., 1998, **37**, 402; (*b*) U. Mitschke and P. Bäuerle, *J. Mater. Chem*., 2000, **10**, 1471.
11 (*a*) C. J. Brabec, N. S. Sariciftci and J. C. Hummelen, *Adv. Funct. Mater*., 2001, **11**, 15; (*b*) S. Roquet, R. D. Bettignies, P. Leriche, A. Cravino and J. Roncali, *J. Mater. Chem*., 2006, **16**, 3040–3045.
12 (*a*) S. Karpe, A. Cravino, P. Frère, M. Allain, G. Mabon and J. Roncali, *Adv. Funct. Mater*., 2007, **17**, 1163; (*b*) R. de Bettignies, Y. Nicolas, P. Blanchard, E. Levillain, J.-M. Nunzi and J. Roncali, *Adv. Mater*., 2003, **15**, 1939.
13 W. Wenseleers, F. Stellacci, T. Meyer-Friedrichsen, T. Mangel, C. A. Bauer, S. J. K. Pond, S. R. Marder and J. W. Perry, *J. Phys. Chem. B*, 2002, **106**, 6853.
14 N. S. Sariciftci, L. Smilowitz, A. J. Heeger and F. Wudl, *Science*, 1992, **258**, 1474.
15 X. Sun, Y. Zhou, W. Wu, Y. Liu, W. Tian, G. Yu, W. Qiu, S. Chen and D. Zhu, *J. Phys. Chem. B*, 2006, **110**, 7702.